Impacts of high-latitude volcanic eruptions on ENSO and AMOC

Francesco S. R. Pausata[a,1], Leon Chafik[a,b,c], Rodrigo Caballero[a], and David S. Battisti[d,e]

[a]Department of Meteorology, Stockholm University and Bolin Centre for Climate Research, 10691 Stockholm, Sweden; [b]National Oceanic and Atmospheric Administration/National Environmental Satellite, Data, and Information Service Center for Satellite Application and Research, College Park, MD 20740; [c]Cooperative Institute for Climate and Satellites, University of Maryland, College Park, MD 20740; [d]Department of Atmospheric Sciences, University of Washington, Seattle, WA 98195; and [e]Uni Research, 5008 Bergen, Norway

Edited by Benjamin D. Santer, Lawrence Livermore National Laboratory, Livermore, CA, and approved September 16, 2015 (received for review May 11, 2015)

Large volcanic eruptions can have major impacts on global climate, affecting both atmospheric and ocean circulation through changes in atmospheric chemical composition and optical properties. The residence time of volcanic aerosol from strong eruptions is roughly 2–3 y. Attention has consequently focused on their short-term impacts, whereas the long-term, ocean-mediated response has not been well studied. Most studies have focused on tropical eruptions; high-latitude eruptions have drawn less attention because their impacts are thought to be merely hemispheric rather than global. No study to date has investigated the long-term effects of high-latitude eruptions. Here, we use a climate model to show that large summer high-latitude eruptions in the Northern Hemisphere cause strong hemispheric cooling, which could induce an El Niño-like anomaly, in the equatorial Pacific during the first 8–9 mo after the start of the eruption. The hemispherically asymmetric cooling shifts the Intertropical Convergence Zone southward, triggering a weakening of the trade winds over the western and central equatorial Pacific that favors the development of an El Niño-like anomaly. In the model used here, the specified high-latitude eruption also leads to a strengthening of the Atlantic Meridional Overturning Circulation (AMOC) in the first 25 y after the eruption, followed by a weakening lasting at least 35 y. The long-lived changes in the AMOC strength also alter the variability of the El Niño–Southern Oscillation (ENSO).

high-latitude volcanic eruptions | AMOC–ENSO interaction | volcanism

Proxy data (1, 2) suggest that the strong reduction of surface insolation over the tropics associated with tropical volcanic eruptions may increase the likelihood of the El Niño–Southern Oscillation (ENSO) and a consequent reduction of the zonal sea surface temperature (SST) gradient along the equatorial Pacific. Modeling studies do not yield consistent results and show both an El Niño-like (3–5) or La Niña-like (6, 7) anomalies following a tropical eruption. Recent studies have also suggested that volcanic eruptions can have a large imprint on ocean circulation, affecting the strength of the Atlantic Meridional Overturning Circulation (AMOC) (8–12) on 5- to 20-y timescales and inducing ocean heat content (OHC) anomalies (13, 14) that may persist for decades. However, this slow recovery has been questioned and may be an artifact of experimental design (15). Furthermore, all previous work on the climate impact of volcanic eruptions has focused on tropical volcanoes; no studies have addressed the potential effects of high-latitude eruptions on ENSO. Here, we use a coupled atmospheric–ocean–aerosol model [Norwegian Earth System Model: NorESM1-M (16, 17)] to identify the mechanisms by which high-latitude volcanic eruptions can impact ENSO behavior in both the short term (up to 2–3 y) and long term (approximately half-century), the latter being mediated by volcano-induced changes in ocean circulation.

We simulate an extreme high-latitude multistage eruption starting on June 1st. We inject 100 Tg of SO_2 and ash—as an analog for the ash injection—mostly into the upper-troposphere/lower stratosphere over a 4-mo period. The eruption is composed of eight injections, each lasting for 4 d and spaced out every 15 d (*SI Appendix*, Table S1). This experimental design was chosen as analog for one of the strongest high-latitude eruptions in historical time, the 1783 Laki eruption in Iceland. The simulated volcanic eruption starts from a specific year selected from a transient historical simulation (1850–2005). An ensemble of simulations (ENS_v) is generated by slightly perturbing the initial conditions of the day of the eruption. In the same fashion, we generate an equivalent no-volcano ensemble (ENS_{nv}) where the volcanic aerosol concentration is set to background conditions (*SI Appendix*). The climate perturbation induced by the volcanic eruption (Δ_v) can be simply expressed as $\Delta_v = STATE_v - STATE_{nv}$, where $STATE_{nv}$ is the unperturbed climate state, and $STATE_v$ is the climate state induced by the eruption. To examine the short-term impact on ENSO, we analyze the simulations described by Pausata et al. (18) in which ENS_{nv} and ENS_v are composed of 20 pairs of simulation, each pair being integrated for 4 y. Here, we extend 10 of these pairs of simulations out to 60 y after the eruption to investigate its long-term impact on the AMOC, OHC, and the spatiotemporal properties of ENSO.

Short-Term Impacts on ENSO

Our results show that the simulated volcanic eruption generates an aerosol plume that is strictly confined to the Northern Hemisphere in the months following the eruption, with no direct radiative forcing on the tropical zone (*SI Appendix*, Fig. S1). Despite this latitudinally restricted forcing, anomalous El Niño-like conditions relative to the no-volcano case appear in the tropical Pacific, peaking between 4 and 9 mo after the beginning of the

Significance

In the model simulations analyzed here, large high-latitude volcanic eruptions have global and long-lasting effects on climate, altering the spatiotemporal characteristic of the El Niño–Southern Oscillation (ENSO) on both short (<1 y) and long timescales and affecting the strength of the Atlantic Meridional Overturning Circulation (AMOC). In the first 8–9 mo following the start of the eruption, El Niño-like anomalies develop over the equatorial Pacific. The large high-latitude eruptions also trigger a strengthening of the AMOC in the first 25 y after the eruption, which is associated with an increase in ENSO variability. This is then followed by a weakening of the AMOC lasting another 30–35 y, associated with decreased ENSO variability.

Author contributions: F.S.R.P. designed and performed research; F.S.R.P. and L.C. analyzed the data; L.C., R.C., and D.S.B. contributed to the interpretation of the model results; F.S.R.P. wrote the paper; and L.C., R.C., and D.S.B. contributed to the writing of the manuscript.

The authors declare no conflict of interest.

This article is a PNAS Direct Submission.

Freely available online through the PNAS open access option.

[1]To whom correspondence should be addressed. Email: francesco.pausata@misu.su.se.

This article contains supporting information online at www.pnas.org/lookup/suppl/doi:10.1073/pnas.1509153112/-/DCSupplemental.

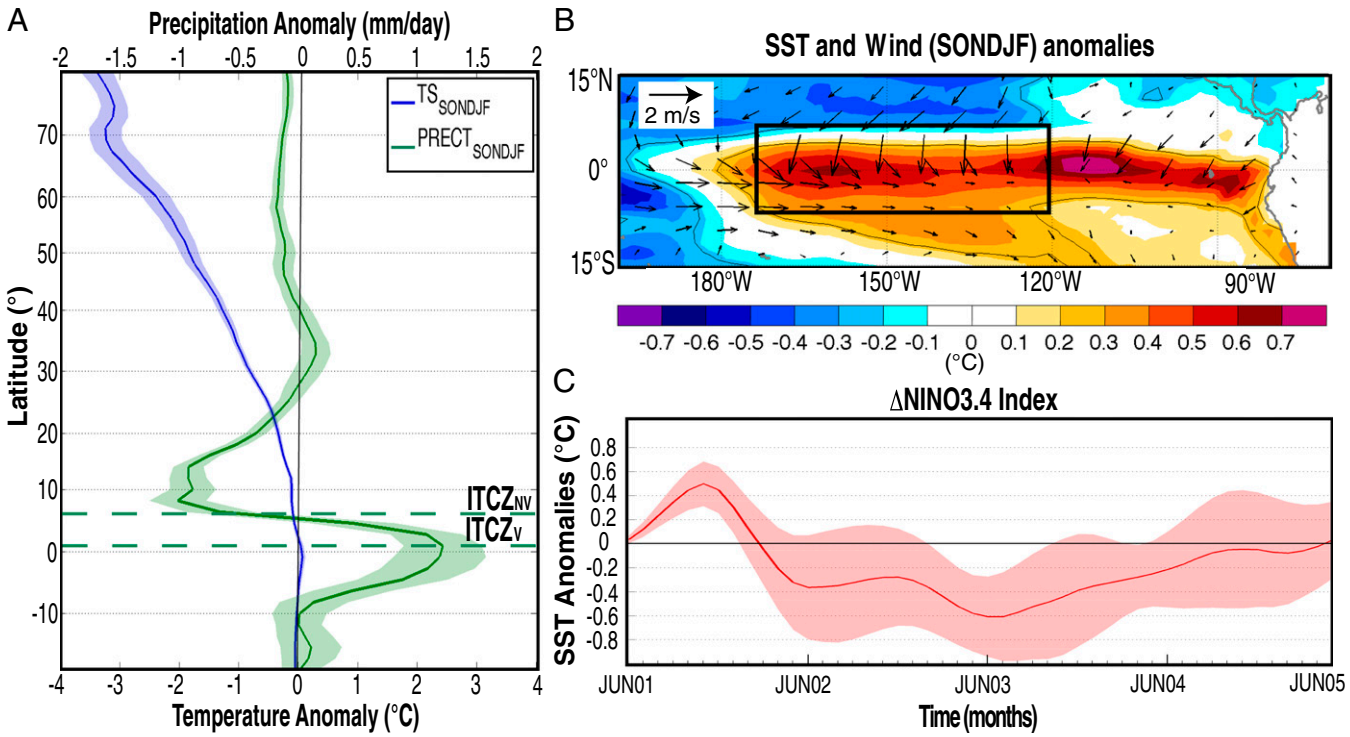

Fig. 1. Temperature, precipitation and wind anomalies following the eruption. (*A*) Ensemble average change (ENS_v minus ENS_{nv}) in the zonal-mean surface temperature (blue) and precipitation (green) over the Pacific basin (150°E to 90°W), for the period 4–9 mo following the start of the eruption (September to February). Shading shows the approximate 95% confidence intervals (twice the SEM) of the change seen in all 20 pairs of experiments. The bold green dashed lines show the ensemble-averaged position of the ITCZ in the no-volcano and volcano simulations. (*B*) Ensemble average changes in near-surface wind (arrows) and SST (shading) 4–9 mo following the start of the eruption. The box shows the Nino3.4 area. The contours delineate the areas where the SST anomalies are significant at the 95% confidence level using a Student *t* test. (*C*) Ensemble average changes in Nino3.4 index due to the eruption.

eruption (Fig. 1 *B* and *C*). The El Niño-like anomaly is followed by cold (La Niña-like) anomalies in the second and third year (Fig. 1*C* and *SI Appendix*, Fig. S5). The El Niño-like anomaly is caused by the strong cooling of the extratropical Northern Hemisphere following the eruption (Fig. 1*A*). It is well established that such interhemispherically asymmetric forcing pushes the Intertropical Convergence Zone (ITCZ) away from the hemisphere that is cooled (19, 20). Hence, the simulated high-latitude eruption causes a southward shift of the ITCZ of ∼5–6° latitude over the Pacific Ocean, bringing the ITCZ closer to the equator during the fall and winter following the eruption (Fig. 1*A* and *SI Appendix*, Figs. S2 and S3). Because surface easterly winds are weakest in the proximity of the ITCZ, this equatorward shift implies a weakening of the easterly winds along the equator in the central and eastern equatorial Pacific (i.e., a westerly anomaly; Fig. 1*B* and *SI Appendix*, Fig. S4). This leads via the Bjerknes feedback (21) to a reduction in the east–west temperature contrast across the tropical Pacific, thus favoring an El Niño-like anomaly. The El Niño-like anomaly is a function of the Northern Hemisphere cooling, but may be influenced by the preexisting ENSO state: a stronger El Niño-like response may develop under La Niña compared with El Niño preexisting conditions (*SI Appendix*, Fig. S5).

In light of our results, we find intriguing that the El Niño event that peaked in January of 1912, 6 mo before the Katmai eruption in June of 1912 (the largest high-latitude eruption of the 20th century), was immediately followed by near-normal conditions in the tropical Pacific rather than the La Niña conditions that normally occur after El Niño events. Another El Niño event occurred a year after the eruption (*SI Appendix*, Fig. S6). Furthermore, tree-ring data (22) suggest that the El Niño conditions preceding the Laki eruption were further strengthened in the winter of 1783–1784 (6–9 mo after the beginning of the eruption), in agreement with our findings. However, further evidence would be needed to test our model results using observations.

Long-Term Impacts on ENSO and AMOC

The impacts of a multistage high-latitude volcanic eruption may not be limited to the first few years following the eruption: our model experiment also shows strong effects on SST variability in the Nino3.4 region and much of the eastern equatorial Pacific that persist for nearly a half-century following the eruption (Fig. 2). Impacts on ENSO frequency, on the other hand, are weak and not statistically discernible (*SI Appendix*, Tables S3 and S4). ENSO variability increases in the first 25 y following the eruption (Fig. 2*A*), whereas it is reduced in the last 35 y of the simulation (years 26–60), particularly between 26 and 45 y after the eruption (Fig. 2*B* and *SI Appendix*, Table S2) after which ENSO variability reverts to normal (Fig. 2*C*).

Along with these changes in ENSO variability, we also find marked changes in the AMOC (Fig. 3*A*). After a brief (<6-mo) weakening of the AMOC, a progressive AMOC strengthening takes place and peaks with a maximum anomaly of about 1.5 sverdrup (Sv) (1 Sv = 10^6 m^3/s) between 5 and 10 y after the eruption (Fig. 3*A*). Thereafter, the AMOC starts to slow down and reaches a minimum (∼1 Sv below that in the unperturbed ensemble) about 35–40 y after the eruption. Although a slow recovery is apparent after this period, the AMOC remains significantly weaker than in the no-volcano ensemble from 25 y after the eruption until the end of the analyzed period. The negative radiative forcing from the volcanic aerosol results in a surface cooling that develops during the first 1–3 y after the eruption (*SI Appendix*, Fig. S8*A*) and is gradually transferred into the deep ocean (Fig. 3*B*). The surface cooling also causes reduced

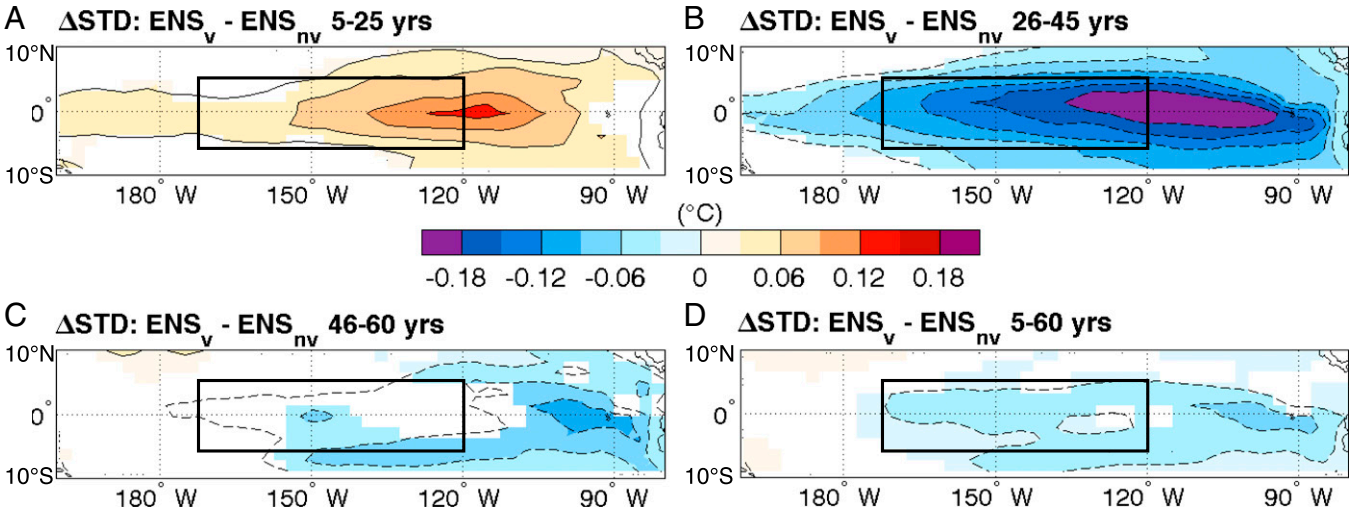

Fig. 2. SST SD changes. Ensemble average change (ENS_v minus ENS_{nv}) in the SD of monthly mean SST (in degrees Celsius) for the period 5–25 y (*A*), 26–45 y (*B*), and 46–60 y (*C*) after the eruption and for the entire time series (*D*). Changes that are significant at the 95% confidence level using an *F* test are shaded. The contour interval is 0.03 °C (dashed, negative anomalies; solid, positive anomalies; the zero line is omitted). We discard the first 4 y to remove the hemispheric-wide cooling due the eruption. The SD is calculated from the concatenated time series using all 10 members in each ensemble. Hence, 210 y of data are used to calculate the SD in *A*: 10 members × 21 y; 200 in *B*, 150 in *C*, and 560 y in *D*. As is commonly done when examining ENSO, we apply a 5-mo running mean on the SST anomalies to damp high-frequency ocean variability unrelated to ENSO. The box shows the Nino3.4 area.

precipitation (*SI Appendix*, Figs. S3 and S8*B*) and consequently reduced river runoff at mid-to-high latitudes of the Northern Hemisphere. Cooler, more saline surface conditions in the first 2 or 3 y (*SI Appendix*, Fig. S9) increase the density of the surface water in the higher latitudes of the Northern Hemisphere that act to destabilize the water column, leading to enhanced oceanic convection in the North Atlantic (*SI Appendix*, Fig. S10) and a spin-up of the AMOC. The strengthening of the AMOC as well as the mechanisms involved are similar to those proposed for tropical eruptions (9, 10): here, we show that the impact on the AMOC is not limited to the first 10–20 y and to tropical eruptions as shown in previous studies (9–11, 23), but can also occur in response to high-latitude eruptions, lasting for 50 y or more.

The changes in ocean circulation are also accompanied by a decrease in the OHC. The eruption immediately cools the surface (*SI Appendix*, Figs. S2 and S8*A*), after which the anomalously cold surface water is transferred into the thermocline layer and deeper in the ocean. Cold anomalies below ∼300 m are established by year 15, and they persist throughout the remainder of the simulation. In this regard, the evolution of the global OHC associated with a high-latitude eruption is similar to

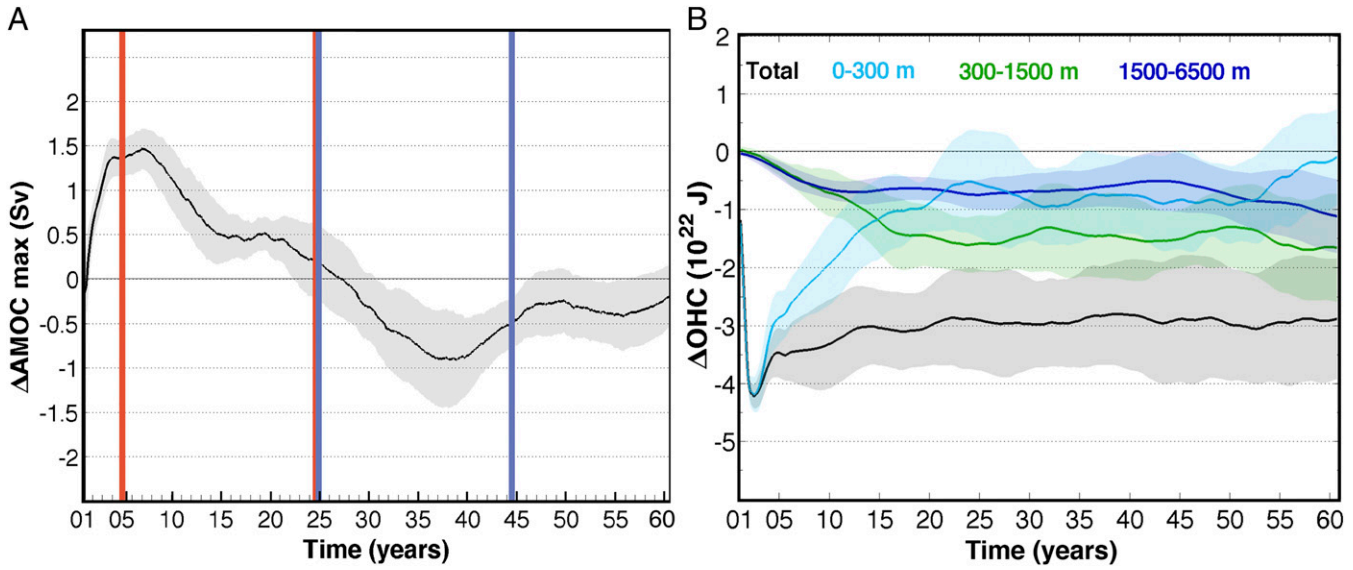

Fig. 3. AMOC index and integrated OHC differences. (*A*) Long-term changes in the AMOC, as indicated by the change in the maximum of the overturning stream function (in sverdrups). The shading shows approximate 95% confidence intervals (twice the SEM) of the difference in all pairs of experiments that comprise the ensembles. The vertical lines bound the periods analyzed in Fig. 2. The mean AMOC strength in the ENS_v is significantly greater (smaller) than that in the ENS_{nv} in the 5–25 (26–45) y after the eruption. We apply a 5-y running mean to the AMOC time series as commonly done in the literature. (*B*) Ensemble average change in OHC (in joules) averaged from the surface to selected depths for the global ocean. Solid lines denote the ensemble average change, and shading represents the SD of the ensemble difference.

that for tropical eruptions such as Tambora, Agung, and Pinatubo (9, 10).

Discussion and Conclusions

In summary, our results illuminate the mechanism by which large summer high-latitude eruptions in the Northern Hemisphere may trigger an El Niño-like anomaly—relative to the no-volcano case—in the first 4–9 mo after the eruption and affect both AMOC and ENSO variability for decades thereafter. Such eruptions generate a hemispheric-scale surface cooling and thus trigger, via energetic constraints (19, 20), a general southward shift in the ITCZ that is particularly marked in the Pacific basin. In turn, the southward-shifted ITCZ in the Pacific generates anomalous surface westerlies over the equatorial western and central Pacific and anomalous equatorial northerlies in the eastern Pacific in the first 4–9 mo following the eruptions (Fig. 1*B*); these anomalies constitute an optimal trigger for an El Niño-like perturbation (24). The processes leading to El Niño-like anomalies in response to high-latitude eruptions are thus very different from those hypothesized to act in response to tropical eruptions (25, 26) and rely on better-understood mechanisms (19, 20). Only a few modeling studies (27–30) have investigated the climate impacts of high-latitude volcanic eruptions, and none has looked at a potential influence on ENSO. Oman et al. (29), using an atmospheric model coupled to a mixed-layer ocean, found a weakening of the summer monsoon circulation and precipitation over Africa and Asia in the summer of the eruption, consistent with our findings. In our model, Northern Hemispheric cooling also gives rise to a southward shift in the Pacific ITCZ and subsequently to an El Niño-like anomaly via a dynamical (Bjerknes) feedback, which is precluded in a mixed-layer ocean model.

Our results also suggest that a large high-latitude eruption has global-scale, long-lasting effects owing to changes in the OHC and the AMOC, which in turn affect ENSO variability. Several modeling and observation-based studies have found a causal link between the AMOC strength and tropical Pacific climate (31–36) through large-scale atmospheric circulation teleconnections associated with SST gradient changes in the tropical Atlantic (*SI Appendix*, Fig. S12). In addition to this atmospheric bridge, a readjustment of the global ocean circulation by oceanic waves also transmits thermocline signals from the North Atlantic to the tropical Pacific (37–39). However, the timescales associated with these teleconnections are very different: the atmospheric influence can be transmitted from the tropical Atlantic into the tropical Pacific in few weeks, whereas the oceanic teleconnections have a timescale of a few decades (36–38).

Studies do not agree on whether ENSO variance is positively or negatively correlated to the AMOC strength. For example, Dong and Sutton (31) and Timmerman et al. (36) examined the response of five climate models to the imposition of freshwater forcing ("hosing") of the North Atlantic Ocean and found a significant increase in ENSO variability when the AMOC was substantially weakened. On the other hand, Timmerman et al. (39) and Atwood (35) show that, in two other models, ENSO variance decreases in response to a hosing of the North Atlantic. The positive correlation between AMOC and ENSO variance is also supported by proxy reconstructions of the impact of the 8.2-ky BP freshwater discharge into the North Atlantic, which shows that the variance of ENSO was reduced for several decades after the freshwater pulse (35). Physically, a stronger AMOC may cause an increase in ENSO variability by shoaling and flattening the Pacific thermocline along the equator (*SI Appendix*, Fig. S13), which enhances the strength of the Bjerknes feedback (*SI Appendix*, Fig. S14) (40).

The lack of robustness of modeled ENSO responses to changes in AMOC is likely the result of the inability to correctly simulate the climatology of the tropical Pacific atmosphere–ocean system, compromising the physics and feedbacks governing the modeled ENSO (41). Analyses of the climate models used in the past decade or so show that in most of them—including in all models (or very similar versions) examined by Timmermann et al. (36)—the spatiotemporal structure of ENSO and the key feedbacks have large biases compared with those observed (42). In contrast, the ENSO simulated by the climate model used here compares favorably to observations [figure 13 in the study by Bellenger et al. (42)] both in terms of mean state (amplitude, spatial structure, frequency spectrum, and the seasonality) and the strength of the feedbacks acting throughout a typical ENSO cycle (the Bjerknes feedback, the heat flux, shortwave and latent heat feedbacks). Our model's more realistic portrayal of key features of ENSO—compared with most climate models—may be related to the fact that the double ITCZ bias over the tropical Pacific—ubiquitous in climate models—is less pronounced in NorESM1-M (16, 17): the simulated ITCZ is more confined to the Northern Hemisphere in NorESM1-M, as observed, rather than being symmetric around the equator as in most of the models.

Our results highlight the potential for large high-latitude eruptions to affect global climate through long-lasting changes in ocean circulation and heat content beyond the lifetime of the injected stratospheric aerosols. Our study also provides new insights for a better understanding of volcanic impacts on ENSO variability, which is of importance also in view of the potential role played by the tropical Pacific in the global warming hiatus (43–47). More generally, our results suggest that multidecadal changes in the AMOC—owing to either natural internal variability or forcing (such as volcanic eruptions)—may modulate the statistics of ENSO for several decades into the future. Further modeling studies, possibly at a community level (48) such as those planned in the Volcano Model Intercomparison Project (49), will be necessary to better assess the robustness and the mechanisms behind the AMOC–ENSO relationship, given the very different AMOC sensitivity to external forcing shown by climate models (14). The potential impact of AMOC modifications on tropical Pacific climate introduces additional challenges in attributing future changes in ENSO variability to changes in human activity.

Materials and Methods

Model Description and Experiment Design. We use the coupled atmospheric–ocean–aerosol model NorESM1-M (16, 17) with horizontal resolution 1.9° (latitude) × 2.5° (longitude) and 26 vertical levels. The model includes treatment of the direct effect of aerosols, and the first and second indirect effects of aerosols on warm clouds. NorESM1 is an Earth System Model that uses a modified version of CAM4, CAM4–Oslo, for the atmospheric part of the model, with an updated module that simulates the life cycle of sea salt, mineral dust, particulate sulfate, black carbon, and primary and secondary organics. CAM4–Oslo is coupled to an updated version of the isopycnal ocean model MICOM. A more detailed description is provided in *SI Appendix*.

The multistage high-latitude eruption is simulated by injecting, mostly in the upper-troposphere/lower stratosphere, 100 Tg of SO_2 and dust over a 4-mo period. The eruption is comprised of eight injections, each lasting for 4 d (*SI Appendix*, Table S1). The simulated volcanic eruption starts from a specific year selected from a transient 156-y historical (1850–2005) simulation. We generate the individual ensemble members by perturbing the initial conditions of the specific year in which the eruption is simulated; perturbations are constructed by replacing the state of the atmosphere on June 1st with that from days immediately preceding or following the eruption. Twenty integrations are performed, each 4 y long. Ten of these integrations are extended to 60 y; together, they constitute the volcanic ensemble, ENS_v. An equivalent ensemble is generated from a control run that has volcanic aerosols set to background conditions (ENS_{nv}): historical aerosol emissions are taken from Intergovernmental Panel on Climate Change AR5 datasets (50). The eruption year selected is the model year 1934 (eruption year: number 01), which is roughly in middle of the climatology period, and it presents El Niño conditions as it was before the Laki eruption (*SI Appendix*). A detailed examination of NorESM performance in interactively

simulating the Laki eruption and a comparison with other modeling studies is available in the study by Pausata et al. (18).

We analyze monthly mean model output. We assess the statistical significance of differences in mean state and variability (at a stipulated 95% significance level) using *t* and *F* tests.

Analyses.

ENSO. The ENSO index used in this study consists of monthly mean SST anomalies spatially averaged over the Nino3.4 region (5°N to 5°S and 170°W to 120°W). A 5-mo running mean is applied to damp uncoupled intraseasonal variations in SST. El Niño events are defined as the periods during which the 5-mo running mean of the SST index anomaly is greater than +0.4 °C for at least 6 consecutive mo. Changes in the ENSO variability are measured as changes in the SST SD in the Nino3.4 area. The SD is calculated from the concatenated time series using all 10 members in each ensemble. The concatenation does not change the variance in ENS_v and ENS_{nv}, and only slightly affects the threshold for statistical significance.

AMOC. The AMOC index is the maximum in the zonally averaged overturning stream function in the North Atlantic between 30°N and 60°N and between 500- and 2,000-m depth. NorESM simulates a vigorous AMOC compared with other models, being in the upper range of AMOC strengths simulated by CMIP3 models (17). Measured by the maximum in the overturning stream function in North Atlantic, the AMOC in the NorESM is about 30 Sv at 26.5°N, whereas the observed AMOC is about 18–20 Sv (1).

ACKNOWLEDGMENTS. We thank A. Hannachi, A. Grini, M. Gaetani, and U. Ninnemann for discussions and suggestions, and J. Carton, A. Robock, and two anonymous reviewers for insightful comments on the manuscript. The simulations were performed on resources provided by the Swedish National Infrastructure for Computing at the National Supercomputer Centre.

1. McGregor S, Timmermann A, Timm O (2010) A unified proxy for ENSO and PDO variability since 1650. *Clim Past* 6(1):1–17.
2. Brad Adams J, Mann ME, Ammann CM (2003) Proxy evidence for an El Niño-like response to volcanic forcing. *Nature* 426(6964):274–278.
3. Mann ME, Cane MA, Zebiak SE, Clement A (2005) Volcanic and solar forcing of the tropical Pacific over the past 1000 years. *J Clim* 18(3):447–456.
4. Ohba M, Shiogama H, Yokohata T, Watanabe M (2013) Impact of strong tropical volcanic eruptions on ENSO simulated in a coupled GCM. *J Clim* 26:5169–5182.
5. Maher N, McGregor S, England MH, Gupta AS (2015) Effects of volcanism on tropical variability. *Geophys Res Lett* 42(14):6024–6033.
6. McGregor S, Timmermann A (2011) The effect of explosive tropical volcanism on ENSO. *J Clim* 24(8):2178–2191.
7. Zanchettin D, et al. (2012) Bi-decadal variability excited in the coupled ocean–atmosphere system by strong tropical volcanic eruptions. *Clim Dyn* 39(1-2):419–444.
8. Otterå OH, Bentsen M, Drange H, Suo L (2010) External forcing as a metronome for Atlantic multidecadal variability. *Nat Geosci* 3(10):688–694.
9. Swingedouw D, et al. (2015) Bidecadal North Atlantic ocean circulation variability controlled by timing of volcanic eruptions. *Nat Commun* 6:6545.
10. Stenchikov G, et al. (2009) Volcanic signals in oceans. *J Geophys Res* 114(D16):D16104.
11. Mignot J, Khodri M, Frankignoul C, Servonnat J (2011) Volcanic impact on the Atlantic Ocean over the last millennium. *Clim Past* 7(4):1439–1455.
12. Zanchettin D, et al. (2013) Background conditions influence the decadal climate response to strong volcanic eruptions. *J Geophys Res Atmos* 118(10):4090–4106.
13. Gleckler PJ, et al. (2006) Volcanoes and climate: Krakatoa's signature persists in the ocean. *Nature* 439(7077):675.
14. Ding Y, et al. (2014) Ocean response to volcanic eruptions in Coupled Model Intercomparison Project 5 (CMIP5) simulations. *J Geophys Res Ocean* 119(9):5622–5637.
15. Gregory JM (2010) Long-term effect of volcanic forcing on ocean heat content. *Geophys Res Lett* 37(22):L22701.
16. Bentsen M, et al. (2013) The Norwegian Earth System Model, NorESM1-M—Part 1: Description and basic evaluation of the physical climate. *Geosci Model Dev* 6(3): 687–720.
17. Iversen T, et al. (2013) The Norwegian Earth System Model, NorESM1-M—Part 2: Climate response and scenario projections. *Geosci Model Dev* 6(2):389–415.
18. Pausata FSR, Grini A, Caballero R, Hannachi A, Seland Ø (2015) High-latitude volcanic eruptions in the Norwegian Earth System Model: The effect of different initial conditions and of the ensemble size. *Tellus B Chem Phys Meterol* 67:26728.
19. Kang SM, Held IM, Frierson DMW, Zhao M (2008) The response of the ITCZ to extratropical thermal forcing: Idealized slab-ocean experiments with a GCM. *J Clim* 21(14):3521–3532.
20. Schneider T, Bischoff T, Haug GH (2014) Migrations and dynamics of the intertropical convergence zone. *Nature* 513(7516):45–53.
21. Bjerknes J (1969) Atmospheric teleconnections from the equatorial Pacific. *Mon Weather Rev* 97(3):163–172.
22. Cook E, Krusic P (2004) *North American Drought Atlas* (NOAA Paleoclimatology Program, Boulder, CO).
23. Iwi AM, Hermanson L, Haines K, Sutton RT (2012) Mechanisms linking volcanic aerosols to the Atlantic Meridional Overturning Circulation. *J Clim* 25(8):3039–3051.
24. Chen Y-Q, Battisti DS, Palmer TN, Barsugli J, Sarachik ES (1997) A study of the predictability of tropical Pacific SST in a coupled atmosphere–ocean model using singular vector analysis: The role of the annual cycle and the ENSO cycle. *Mon Weather Rev* 125(5):831–845.
25. Hirono M (1988) On the trigger of El Niño Southern Oscillation by the forcing of early El Chichón volcanic aerosols. *J Geophys Res* 93(D5):5365.
26. Clement AC, Seager R, Cane MA, Zebiak SE (1996) An ocean dynamical thermostat. *J Clim* 9(9):2190–2196.
27. Highwood EJ, Stevenson DS (2003) Atmospheric impact of the 1783–1784 Laki Eruption: Part II. Climatic effect of sulphate aerosol. *Atmos Chem Phys* 3:1177–1189.
28. Oman L, Robock A, Stenchikov GL, Schmidt GA, Ruedy R (2005) Climatic response to high-latitude volcanic eruptions. *J Geophys Res* 110(D13):D13103.
29. Oman L, Robock A, Stenchikov GL, Thordarson T (2006) High-latitude eruptions cast shadow over the African monsoon and the flow of the Nile. *Geophys Res Lett* 33(18): L18711.
30. Kravitz B, Robock A (2011) Climate effects of high-latitude volcanic eruptions: Role of the time of year. *J Geophys Res* 116(D1):D01105.
31. Dong B, Sutton RT (2007) Enhancement of ENSO variability by a weakened Atlantic thermohaline circulation in a coupled GCM. *J Clim* 20(19):4920–4939.
32. Dong B, Sutton RT, Scaife AA (2006) Multidecadal modulation of El Niño–Southern Oscillation (ENSO) variance by Atlantic Ocean sea surface temperatures. *Geophys Res Lett* 33(8):L08705.
33. Dong B-W, Sutton RT (2002) Adjustment of the coupled ocean-atmosphere system to a sudden change in the thermohaline circulation. *Geophys Res Lett* 29(15):18-1–18-4.
34. Zhang R, Delworth TL (2005) Simulated tropical response to a substantial weakening of the Atlantic thermohaline circulation. *J Clim* 18(12):1853–1860.
35. Atwood AR (2015) Mechanisms of tropical Pacific climate change during the Holocene. PhD dissertation (University of Washington, Seattle).
36. Timmermann A, et al. (2007) The influence of a weakening of the Atlantic Meridional Overturning Circulation on ENSO. *J Clim* 20(19):4899–4919.
37. Goodman PJ (2001) Thermohaline adjustment and advection in an OGCM*. *J Phys Oceanogr* 31(6):1477–1497.
38. Cessi P (2004) Global seiching of thermocline waters between the Atlantic and the Indian-Pacific Ocean Basins. *Geophys Res Lett* 31(4):L04302.
39. Timmermann A, An S-I, Krebs U, Goosse H (2005) ENSO suppression due to weakening of the North Atlantic thermohaline circulation. *J Clim* 18(16):3122–3139.
40. Russell AM, Gnanadesikan A (2014) Understanding multidecadal variability in ENSO amplitude. *J Clim* 27(11):4037–4051.
41. Neelin JD, et al. (1998) ENSO theory. *J Geophys Res* 103(C7):14261.
42. Bellenger H, Guilyardi E, Leloup J, Lengaigne M, Vialard J (2014) ENSO representation in climate models: From CMIP3 to CMIP5. *Clim Dyn* 42(7-8):1999–2018.
43. England MH, et al. (2014) Recent intensification of wind-driven circulation in the Pacific and the ongoing warming hiatus. *Nat Clim Chang* 4(3):222–227.
44. Chen X, Tung K-K (2014) Climate. Varying planetary heat sink led to global-warming slowdown and acceleration. *Science* 345(6199):897–903.
45. Santer BD, et al. (2015) Observed multivariable signals of late 20th and early 21st century volcanic activity. *Geophys Res Lett* 42(2):500–509.
46. Santer BD, et al. (2014) Volcanic contribution to decadal changes in tropospheric temperature. *Nat Geosci* 7(3):185–189.
47. Maher N, Sen Gupta A, England MH (2014) Drivers of decadal hiatus periods in the 20th and 21st centuries. *Geophys Res Lett* 41(16):5978–5986.
48. Pausata FSR (2015) How do high-latitude volcanic eruptions affect climate? *Eos* 96. Available at https://eos.org/meeting-reports/how-do-high-latitude-volcanic-eruptions-affect-climate. Accessed March 15, 2015.
49. World Climate Research Programme, VolMIP: Model Intercomparison Project on the climate response to Volcanic forcing. Available at www.wcrp-climate.org/index.php/modelling-wgcm-mip-catalogue/modelling-wgcm-mips/505-modelling-wgcm-volmip. Accessed July 12, 2015.
50. Kirkevåg A, et al. (2013) Aerosol-climate interactions in the Norwegian Earth System Model—NorESM1-M. *Geosci Model Dev* 6:207–244.